Proceedings of FEDSM'98
1998 ASME Fluids Engineering Division Summer Meeting
June 21-25, 1998, Washington, DC, USA

FEDSM98-5042

VOID FRACTION MEASURMENT BENEATH A STATIONARY BREAKING WAVE

Tricia A. Waniewski*, Christopher E. Brennen, and Fredric Raichlen
Division of Engineering and Applied Science
California Institute of Technology
Pasadena, California 91125
Email: waniewsk@plesset.caltech.edu

ABSTRACT

Impedance based techniques have been used to quantify air entrainment by a stationary breaking wave at the bow of a ship. The present paper describes an impedance based void fraction meter which was developed to make measurements in this high speed, unsteady, multiphase flow, and details of its calibration are provided. In addition, air entrainment data from an experimental simulation of a bow wave are presented. The local, time averaged void fraction was mapped for flow cross sections beneath the plunging wave jet, revealing the location of the clouds of bubbles formed by that jet impacting the incoming water surface. Size distribution functions for the bubbles within the bubble clouds are also presented. The results are correlated with the wave structure described in Waniewski et al. (1997).

NOMENCLATURE

- A IVFM measurement cross sectional area (m^2)
- d Depth (m)
- $\mathbf{F}$ Froude number based on depth, $\mathbf{F} = U/\sqrt{gd}$
- g Gravitational acceleration (m/s^2)
- l Bubble chord length (mm)
- N Bubble count rate ($counts/s$)
- U Free stream velocity (m/s)
- x Streamwise coordinate (cm)
- y Cross stream coordinate (cm)
- z Vertical coordinate (cm)

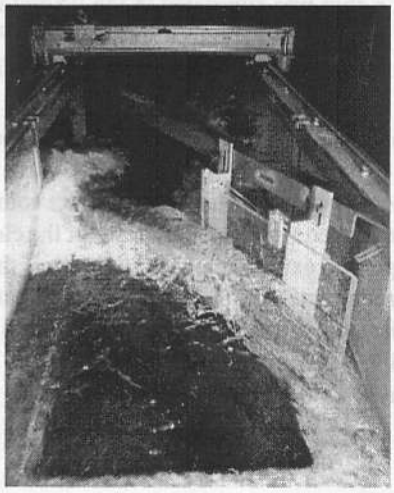

Figure 1. PHOTOGRAPH OF THE TEST SECTION VIEWED FROM UPSTREAM; $\theta = 13.4°$, $\phi \approx 15°$, $U = 2.45m/s$, $d = 11.45cm$, AND $\mathbf{F} = 2.31$

- α Void fraction (%)
- ϕ Dihedral angle (degrees)
- θ Wedge half angle (degrees)

INTRODUCTION

In flows around ships, a breaking bow wave entrains air as its jet impinges continuously on the free surface. The resulting

*Address all correspondence to this author.

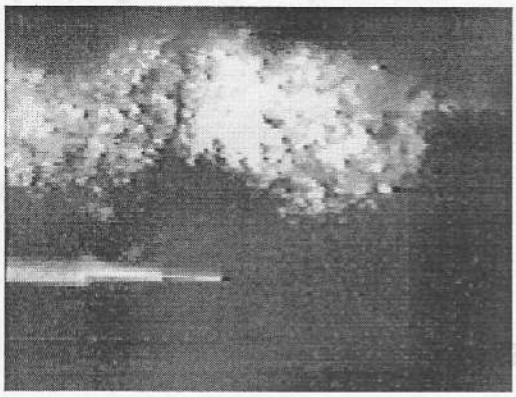

Figure 2. HIGH SPEED VIDEO LOOKING BENEATH THE FREE SURFACE AT BUBBLE CLOUDS PASSING BY THE TIP OF THE IVFM PROBE. THE FLOW IS FROM RIGHT TO LEFT AND THE PROBE IS LOCATED BENEATH THE IMPACTING BOW WAVE JET; $\theta = 25°, \phi = 0°$, $U = 1.83m/s, d = 8.01cm$, AND $\mathbf{F} = 2.06$.

air bubbles persist in the ship wake affecting its radar cross section as well as acting as cavitation nuclei in the flow entering the ship's propeller. In the present investigation, the formation of a bow wave on a ship was simulated in the laboratory using a deflecting plate in a supercritical free surface flow. Figure 1 shows the experimental set up and details are given in Waniewski et al. (1997).

Photographs show that the air is entrained as periodic bubble clouds and an example is shown in Figure 2. These bubble clouds have a diameter of approximately 5 cm and are comprised of bubbles which are packed tighter at the center of the cloud than at the edges. In the present experimental configuration, the clouds seem to grow in size at a steady rate until they encounter the bottom and/or opposite wall of the flume facility. Bubble size, velocity, and void faction were measured using high speed videos and an impedance based void fraction meter (IVFM).

DESIGN OF IVFM

Unsteady dynamic void fraction measurements by impedance based techniques have been conducted successfully by many researchers since the seminal work of Cimorelli and Evangelisti (1969), Garrard and Ledwidge (1971), and Jallouk et al (1979). These include Bernier (1982) and Chanson (1988) among others. The IVFM discussed herein is different since it does not measure the average void fraction over a measurement volume but rather detects bubbles at a particular point to define a local void fraction. The design described in the following sections is simple, low cost, has a good dynamic response, and is robust in high speed flow conditions, all requirements for the ship bow wave measurements.

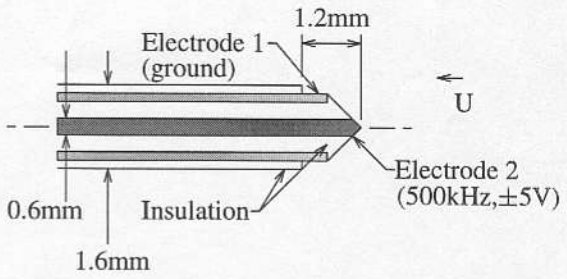

Figure 3. CROSS-SECTIONAL VIEW OF THE IVFM PROBE, NOT TO SCALE.

Probe design

The IVFM probe which consists of two concentric stainless steel electrodes is based on a design by Chanson (1988) and is shown in Figure 3. The outer annular electrode is a syringe needle; the inner electrode is a wire with a diameter of 0.6 mm. Epoxy fills the gap between the two electrodes and insulates them from each other. Also, the outer electrode is insulated from the water except for a length of approximately 0.5 mm from the tip. The probe has a sharpened tip to avoid flow separation and is mounted on a support system downstream of the probe.

The probe's small size allows it to respond to individual bubbles. Experiments with larger probes of this style did not produce desirable signal to noise ratios. Parallel plate style probes tested for use had grounding loop and vibration problems; they also entrained air in the separation zones generated by the plates.

The probe is attached to a carriage, visible at the top of Figure 1, which travels on precision rails mounted to the top of the flume sidewalls. It can be moved in the cross-stream and downstream directions by two servo motors controlled by a PC.

Electronic design

The electronics associated with the IVFM detects small changes in the fluid impedance of the water immediately surrounding the probe. An oscillator is used to generate a sinusoidal voltage signal of $\pm$ 5V and 500 kHz which, after passing through a buffer, is applied to the inner electrode. The outer electrode is grounded. When a bubble passes the probe tip, the current flowing between the two electrodes is reduced, and a current meter is used to measure this change. The output is then low-pass filtered with a cutoff of 40 kHz and demodulated to provide a DC signal proportional to the local void fraction. The resulting DC signal from the IVFM is sampled using a data acquisition system with a data collection rate between 2 kHz and 20 kHz depending on the bubble velocity.

SINGLE BUBBLE TESTS

Single bubble tests were performed to determine the sensitivity of the probe to bubble position. The probe was mounted

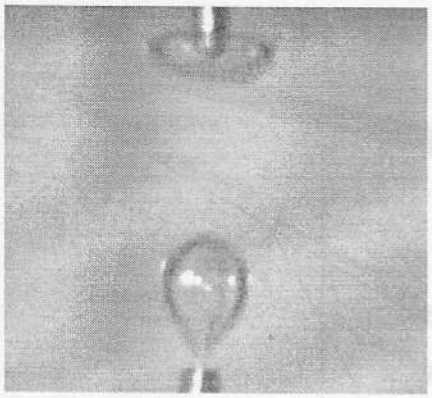

Figure 4. HIGH SPEED VIDEO OF SINGLE BUBBLE TEST SETUP. ONCE THE BUBBLES DETACH FROM THE TUBING, THEY TRAVEL UPWARDS WITH A VELOCITY OF $0.27m/s$, AND IMPACT THE PROBE TIP AS AN OBLATE SPHEROID SHOWN AT THE TOP.

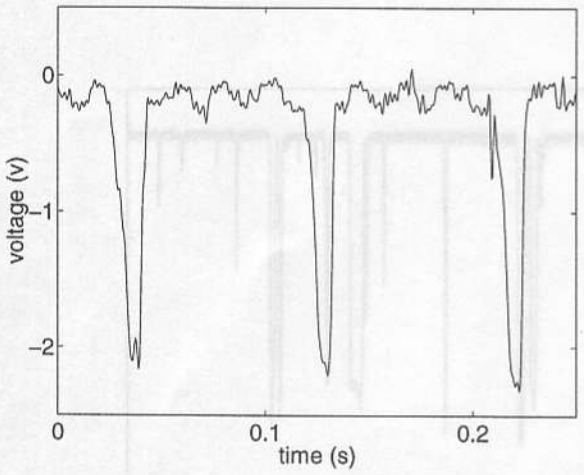

Figure 5. TYPICAL IVFM SIGNAL FROM THE SINGLE BUBBLE TESTS. EACH LARGE NEGATIVE SPIKE CORRESPONDS TO AN AIR BUBBLE IMPACTING THE PROBE TIP.

in a small aquarium with the tip pointing downward. A small air pump was connected to a 1.66 mm diameter stainless steel tube installed several centimeters below the probe tip. The air flow rate was adjusted so that single bubbles were intermittently released from the stainless steel tube. The bubbles were of uniform 5 mm diameter just before release and deformed as they traveled upward as shown in Figure 4. The high speed video camera and the IVFM data acquisition system were triggered simultaneously. Figure 5 shows a typical signal. Correlation of the images with these signals confirmed that a large negative spike is produced each time a bubble impacts the probe, although the spike amplitude and spike width were shown to be sensitive to the lateral location of the bubble at impact.

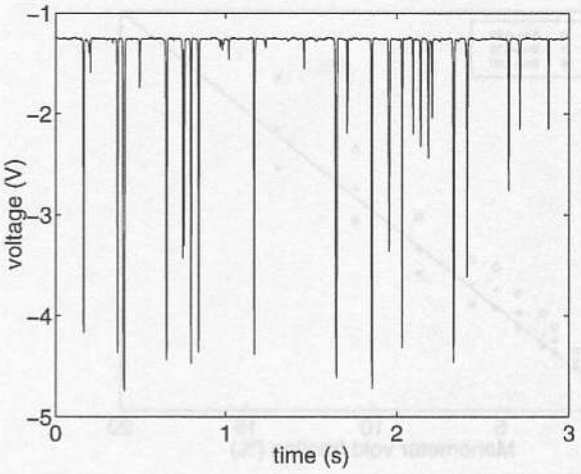

Figure 6. TYPICAL IVFM SIGNAL FROM THE CALIBRATION EXPERIMENTS. A VOLTAGE OF -1.2 V OCCURS WHEN NO BUBBLES ARE TOUCHING THE PROBE TIP AND EACH LARGE NEGATIVE SPIKE CORRESPONDS TO AN AIR BUBBLE PASSING BY THE PROBE TIP.

CALIBRATION OF IVFM

A two phase flow facility was used to calibrate the IVFM. This facility included a vertical lucite pipe 10.16 cm in diameter with an air injector located 1 m below the IVFM probe. The injector produced air bubbles of uniform size with a diameter of roughly 5 mm, and the air flow rate was adjustable. Two static pressure taps located 1.1 m apart, and approximately equally spaced above and below the IVFM probe, were connected to an inverted manometer whose reading was used to obtain the steady state void fraction, α. High speed videos of these flows were also obtained.

A typical signal from the IVFM corresponding to $\alpha = 4.31\%$ from the IVFM is shown in Figure 6. Each of the spikes is well defined. The high speed videos confirmed that each spike corresponded with the impact of a bubble on the probe tip. The IVFM signals were post-processed using software. Since the sampling rate was 2 kHz, a fourth order Butterworth filter with a cutoff frequency of 1 kHz (the Nyquist frequency) was used to eliminate any parts of the signal that had a non-physical origin. Forward and reverse filtering yielded zero-phase distortion. To compensate for any drift of the IVFM electronics, the mean noise level was subtracted from each signal.

Void fraction was calculated from the conditioned signals, using

$$\overline{\alpha(\mathbf{x},\tau)} = \frac{1}{\tau}\int_0^\tau M(\mathbf{x},t)dt \qquad (1)$$

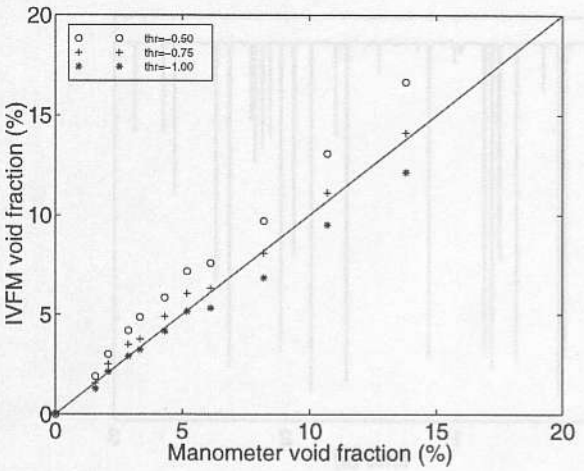

Figure 7. CALIBRATION CURVE FOR THE IMPEDANCE BASED VOID FRACTION METER FROM THE TWO PHASE FLOW FACILITY. THE LINEAR CURVE FIT FOR THE DATA CORRESPONDING TO thr = -0.75 V IS y = 1.00x + 0.32.

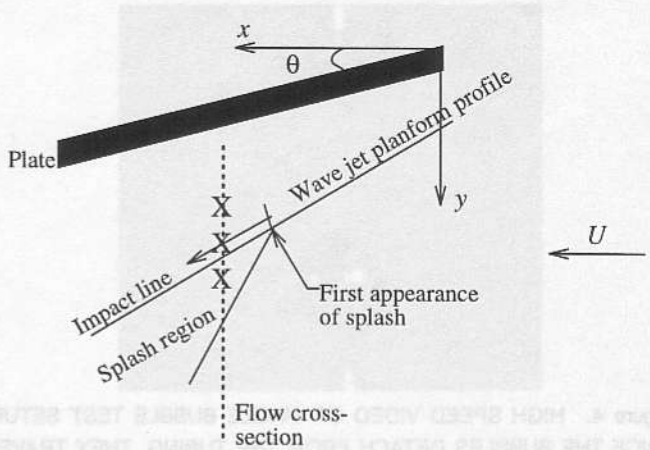

Figure 8. SCHEMATIC DIAGRAM OF THE FLOW FEATURES WITH A TYPICAL FLOW CROSS SECTION INDICATED. THE IVFM PROBE TRAVELS ALONG THESE CROSS SECTIONS AND SAMPLES ARE TAKEN AT POSITIONS SUCH AS THOSE MARKED 'X' FOR DIFFERENT DEPTHS.

where $\mathbf{x}$ is the measurement point, and τ is the integration time (Ishii, 1975). The value of $M(\mathbf{x},t)$ is either 0 or 1 depending on whether the signal exceeded a chosen threshold or not and therefore indicates whether the probe was registering the presence of a bubble (or not). Similar procedures have been used by other researchers using conductivity probes to measure void fraction. For example, Teyssedou et al. (1988) reported good agreement between void profiles obtained by their conductivity probe and an optical probe.

The calibration was repeated on four different days, and a typical calibration curve is shown in Figure 7. The void fractions were estimated using three different thresholds, and a threshold of -0.75V was shown to give the estimate closest to the measured value, especially at the lower void fractions. This threshold was then used for determining void fraction in the simulated bow wave experiments.

EXPERIMENTAL RESULTS

For measurements in the simulated bow wave, the probe was mounted on the carriage as shown in Figure 1. Samples were taken at different cross-sections in the impact line region of the flow as illustrated in Figure 8. A typical signal from the IVFM located directly beneath the impacting bow wave jet is shown in Figure 9. The IVFM signals were sampled at 20kHz, three times for each location. Simultaneous high speed video (500 fps) was taken with the field of view illuminated by a stroboscope triggered by the camera. The signals were carefully compared with the high speed video images, and it was found that individual bubbles within the bubble cloud produced spikes as they impacted the

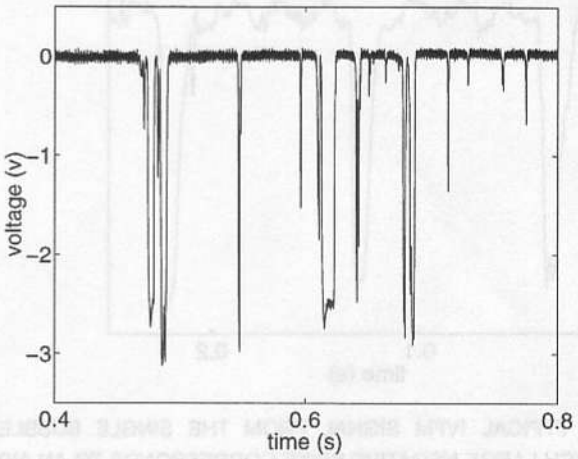

Figure 9. TYPICAL SIGNAL FROM THE IVFM LOCATED SEVERAL cm BENEATH THE BOW WAVE JET; ; $\theta = 26°$, $\phi = 0°$, $U = 2.39m/s$, $d = 6.47cm$, AND $\mathbf{F} = 3.00$. USING THE CALIBRATION CURVE, THE TIME AVERAGED VOID FRACTION, $\alpha \approx 6.5\%$.

probe. The signals were then processed as described in the preceding section to obtain the local, time-averaged void fraction, and the calibration shown in Figure 7 for thr = -0.75 V was applied.

Examples of time averaged void fraction mappings in the impact region of the plunging wave jet are shown in Figure 10. For each figure, the leading edge of the deflecting plate is located at $(x,y) = (0,0)$ and the upstream free surface is located at $z = 0$. On average, the sampling grids for the cross section contained 20 lo-

cations. Because the free surface is unsteady, it was not possible to estimate void fractions at locations above $z = -1$ cm without the free surface dipping below the probe, or the probe entraining air from above the free surface.

These figures confirm several observations from the high speed video. First, the bubble clouds are shown to be roughly spherical in shape and grow as they convect downstream. Second, the greater void fractions at the center of the cloud support the observation that the bubbles are more tightly packed at the cloud center than at the edges. These void fraction mappings will be used to estimate the rate of air entrainment by the wave for different flow conditions.

Bubble chords were calculated by multiplying the individual spike widths from the IVFM signals by the mean flow velocity (for very small bubbles this chord would be close to the bubble diameter). Then the IVFM signals were used to produce bubble chord distributions for the bubbles which comprise the bubble clouds. Figure 11 includes distributions for bubble clouds located at the cross-section shown in Figure 10e. Most bubble chords were $1 \rightarrow 7$ mm (consistent with high speed video observations of the bubbles), and the number of these bubbles increase from the edge to the center of the cloud and from the bottom to the top of the cloud. In addition, larger pockets of air exist in the center of the cloud near the free surface, giving rise to the larger bubble chords registered. The larger pockets of air do not persist in the clouds; they are either broken up into smaller bubbles by the turbulent flow or rise to the free surface.

The center of the cloud, or the region with greatest void fraction, was located directly beneath the impacting plunging wave jet. These distribution data were limited by the depth of water in the flume; distributions at depths greater than $z = -4$ cm are affected by the bottom. For this reason, the distribution data are confined to locations nearer to the free surface and provide information on the initial stages of air entrainment.

DISCUSSION

The preceeding section presents the time-averaged void fractions and bubble distributions; however, study of the fluctuations in void fraction are equally important especially in understanding the air entrainment process for this type of wave. Waniewski et al. (1997) described surface disturbances on the plunging face of the bow wave as "almost equally spaced striations" and "the edge of the breaking wave is very rough and appears almost to be comprised of individual jets". Furthermore, it was "suspected that the periodicity of the bubble clouds is related to the periodicity of the observed surface irregularities". This hypothesis will be investigated through analysis of the unsteady component in the void fraction measurements. In particular, recent study of these disturbances using special flush mounted gages providing water surface time histories showed that indeed they convect downstream with a particular wavelength, and it may be possible to correlate these signals to those taken by the IVFM.

CONCLUSIONS

A simple impedance based void fraction meter with a dynamic response of 40 kHz was designed to quantify the air entrained by a breaking wave. Signals produced by the instrument were interpreted using high speed video images. A special two phase flow facility was used to calibrate the instrument, and it has been used to successfully determine the local, time averaged void fraction associated with air entrained in an experimentally simulated bow wave. Void fraction mappings beneath the plunging wave jet show the path of the bubble clouds, and their bubble chord distributions have also been measured.

ACKNOWLEDGMENT

The authors wish to acknowledge Dr. Steven Ceccio for assistance in developing the IVFM electronics, Hai Vu for assistance in developing the electronics and the IVFM probe, Dr. Sudipto Sur for assistance with signal processing, and Dr. Roberto Zenit for assistance with the two phase flow test facility. They are also grateful for the support of the Office of Naval Research under grant number N00014-94-1-1210.

REFERENCES

Bernier, R., "Unsteady Two Phase Flow Instrumentation and Measurement", Ph.D. thesis, Division of Engineering and Applied Science, California Institute of Technology, 1982.

Bonetto, F. and Lahey, R.T., "An Experimental Study on Air Carry Under Due to a Plunging Liquid Jet", Journal of Multiphase Flow, 19, 1993, 281-294.

Chanson, H., Air Bubble Entrainment in Free Surface Turbulent Flows, Department of Civil Engineering at the University of Queensland, Report CH46/95, 1995.

Chanson, H. and Cummings, P.D., "Modeling Air Entrainment in Plunging Breakers", International Symposium on Waves–Physical–Numerical Modeling, Vancouver 1994.

Chanson, H., "A Study of Air Entrainment and Aeration Devices on a Spillway Model", PhD thesis, Ref. 88-8, Dept. of Civil Engrg., Univ. of Canterbury, New Zealand, 1988.

Cimorelli, L. and Evangelisti, R., "Experimental Determination of the Slip Ratio in a Vertical Boiling Channel Under Adiabatic Conditions at Atmospheric Pressure", International Journal of Heat and Mass Transfer, 12, 1969, 713-726.

Cipriano, R.J. and Blanchard, D.C., "Bubble and Aerosol Spectra Produced by a Laboratory Breaking Wave", Journal of Geophysical Research, 86, 1981, 8085-8092.

Garrard, G. and Ledwidge, T.J., "Measurement of Slip Distortion and Average Void Fraction in an Air Water Mixture",

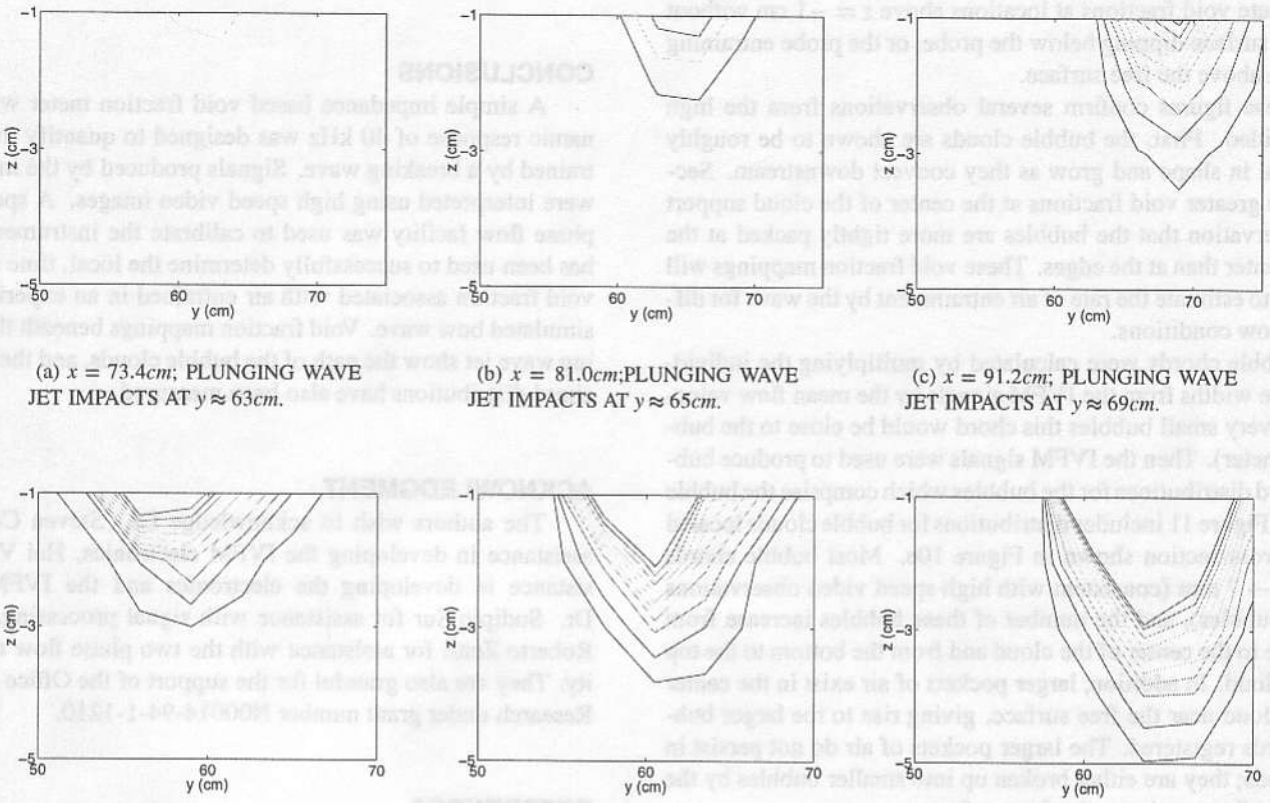

(a) $x = 73.4cm$; PLUNGING WAVE JET IMPACTS AT $y \approx 63cm$.

(b) $x = 81.0cm$;PLUNGING WAVE JET IMPACTS AT $y \approx 65cm$.

(c) $x = 91.2cm$; PLUNGING WAVE JET IMPACTS AT $y \approx 69cm$.

(d) $x = 70.8cm$; PLUNGING WAVE JET IMPACTS AT $y \approx 56cm$.

(e) $x = 75.9cm$;PLUNGING WAVE JET IMPACTS AT $y \approx 60cm$.

(f) $x = 84.2cm$; PLUNGING WAVE JET IMPACTS AT $y \approx 64cm$.

Figure 10. LOCAL, TIME AVERAGED VOID FRACTION FOR THREE DIFFERENT FLOW CROSS SECTIONS AS VIEWED FROM DOWNSTREAM BENEATH THE BREAKING WAVE. FOR (a), (b), AND (c), $\theta = 26°$, $\phi = 0°$, $U = 2.48m/s$, $d = 7.89cm$, AND $\mathbf{F} = 2.82$. FOR (d), (e), AND (f) $\theta = 26°$, $\phi = 0°$, $U = 2.39m/s$, $d = 6.47cm$, AND $\mathbf{F} = 3.00$. TEN EQUALLY SPACED CONTOUR LEVELS BETWEEN VOID FRACTIONS OF 1% AND 10% ARE SHOWN, WITH VOID FRACTION = 1% ON THE OUTER EDGE OF THE BUBBLE CLOUD.

Australia Atomic Energy Research Establishment, 1971, Lucas Heights, Sutherland, N.S.W.

Ishii, M., Thermo-Fluid Dynamic Theory of Two-Phase Flow, Eyrolles, Paris, 1975.

Jallouk, P.A., Leavell, W.H., Shahrokhi, F., and J.E. Hardy, "Advanced Instrumentation for Reflood Studies", Proc. of the U.S. Nuclear Regulatory Commission, Review Group Meeting on Two Phase Flow Instrumentation, March 1979, Troy N.Y. (NUREG/CP-0006).

Lamarre, E. and Melville, W.K., "Air Entrainment and Dissipation in Breaking Waves", Nature, 351, 1991, 469-472.

Loewen, M.R., O'Dor, M.A., and Skafel, M.G., "Bubbles Entrained by Mechanically Generated Breaking Waves", Journal of Geophysical Research, 101, 1996, 20759-20769.

Teyssedou, A., Tapucu, A., and Lortie, M., "Impedance probe to measure local void fraction profiles", Review of Scientific Instruments, 59(4), 1988, 631-638.

Waniewski, T.A., Brennen, C.E., and Raichlen, F., "Experimental Simulation of a Bow Wave", Proc. ASME Fluids Engineering Division Summer Meeting, Symposium on Gas-Liquid Two Phase Flows, 1997.

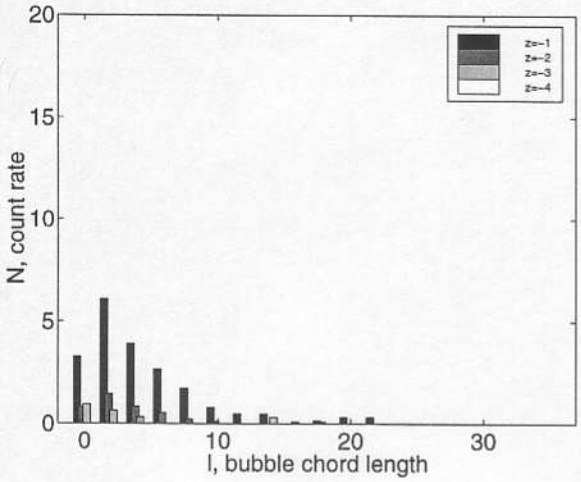

(a) $x = 75.9cm, y = 66.6cm$

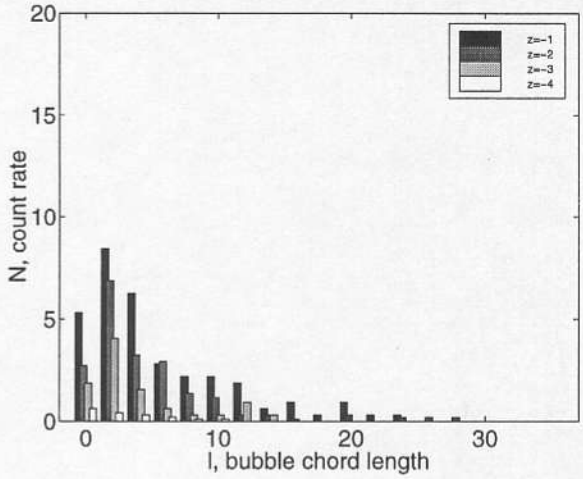

(b) $x = 75.9cm, y = 63.5cm$

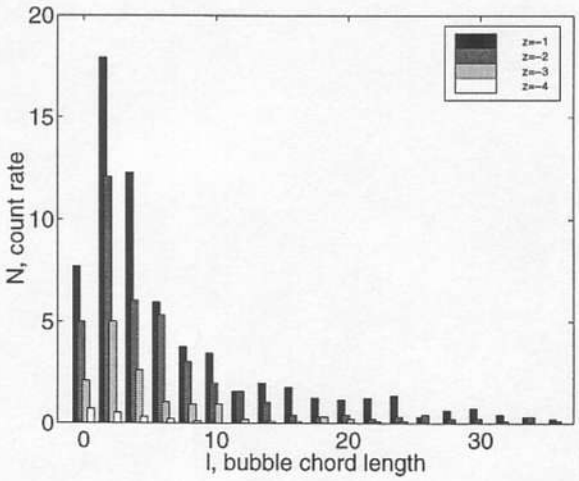

(c) $x = 75.9cm, y = 60.5cm$

Figure 11. BUBBLE CHORD DISTRIBUTIONS FROM BUBBLE CLOUDS OBSERVED BENEATH THE BREAKING WAVE. EACH SUBFIGURE PRESENTS DISTRIBUTIONS FOR FOUR DIFFERENT DEPTHS $z = -1cm$, $z = -2cm$, $z = -3cm$. and $z = -4cm$. THE FLOW CONDITIONS ARE THE SAME AS THOSE FOR FIGURE 10d,e,f.